

Single-objective selective-volume illumination microscopy enables high-contrast light-field imaging

SARA MADAAN,^{1,*}† KEVIN KEOMANEE-DIZON,^{1,*} MATT JONES,²
CHENYANG ZHONG,¹ ANNA NADTOCHIY,¹ PETER LUU,² SCOTT E. FRASER,¹ THAI V.
TRUONG^{2,§}

¹Translational Imaging Center, Dornsife College of Letters, Arts and Sciences, and Viterbi School of Engineering, University of Southern California, Los Angeles, CA 90089, USA

²Translational Imaging Center, Molecular and Computational Biology Section, Department of Biological Sciences, University of Southern California, Los Angeles, CA 90089, USA

*These authors contributed equally to this work

†Present address: Google Inc, Mountain View, CA 94043, USA

§Corresponding author: tvtruong@usc.edu

The performance of light-field microscopy is improved by selectively illuminating the relevant subvolume of the specimen with a second objective lens [1-3]. Here we advance this approach to a single-objective geometry, using an oblique one-photon illumination path or two-photon illumination to accomplish selective-volume excitation. The elimination of the second orthogonally oriented objective to selectively excite the volume of interest simplifies specimen mounting; yet, this single objective approach still reduces out-of-volume background, resulting in improvements in image contrast, effective resolution, and volume reconstruction quality. We validate our new approach through imaging live developing zebrafish, demonstrating the technology's ability to capture imaging data from large volumes synchronously with high contrast, while remaining compatible with standard microscope sample mounting.

Biological processes often depend on the tight spatiotemporal coordination between cells across tissue-level length scales, extending over hundreds of microns in three-dimensions (3D). Functional understanding of such processes would be greatly aided by imaging tools that offer the combined speed and sensitivity needed to observe 3D cellular dynamics without compromising the normal biology [4,5]. Light-field microscopy (LFM) is a fast, synchronous 3D imaging technique [6-8]. Unlike popular volumetric imaging methods that reconstruct a 3D image from intensity information collected one voxel, one line, or one plane at a time, LFM captures both the 2D spatial and 2D angular information of light emitted from the sample [Fig. 1(A)], permitting computational reconstruction of the signal from a full volume in just one shot. Because lateral spatial resolution must be

compromised to capture the angular distribution of the emitting light to yield the extended depth coverage, LFM sacrifices some resolution for its dramatically increased acquisition speed. While 3D deconvolution can be used to enhance LFM performance [7,8], out-of-volume fluorescence background, coming from parts of the sample outside of the volume of interest, limits signal detection, image contrast and resolution. Conventional wide-field illumination excites significant out-of-volume background [Fig. 1(B)], especially for volumes within thick or densely fluorescent samples, precluding LFM's full potential in intact tissues.

We recently introduced an improved light-field-based imaging approach, selective-volume illumination microscopy (SVIM), where confining excitation preferentially to the volume of interest reduces extraneous out-of-volume background, thereby sharpening image contrast, reducing unwanted photodamage, and improving the *effective* resolution in thick specimens (hundreds of microns or more) [1,3]. SVIM was implemented with two objective lenses: one to selectively illuminate the volume of interest, and a second objective, orthogonally aligned, to acquire the fluorescent light-field [Fig. 1(C)]. This two-objective geometry requires that the sample be mounted within the mutual intersecting volume defined by the perpendicular objectives, complicating sample mounting and limiting sample size. Here, we implement SVIM in a single-objective geometry, eliminating the need for two orthogonally oriented objectives, greatly simplifying sample mounting and broadening its utility for biological research.

This new technique, termed axial single-objective SVIM (ASO-SVIM), selectively illuminates the sample volume through the same objective used for high-numerical-aperture (NA) detection (Supplement 1, Section 1, and Fig. S1). The volume of interest is preferentially excited by either one-photon or two-photon processes (1P- or 2P-ASO-SVIM). 1P-ASO-SVIM is accomplished by using a 2D light-sheet oriented obliquely to the axial axis [Fig. 1(D)], created via a cylindrical lens; the sample is illuminated by sweeping this oblique sheet in 1D to excite fluorescence within the desired region of interest, multiple times within a single

camera exposure. 2P-ASO-SVIM [Fig. 1(E)] is accomplished using a low-NA Gaussian beam that is raster-scanned in 2D to excite the 3D sample volume of interest.

To capture fluorescence light-fields emitted from the excited volume, a lenslet array is placed at the native image plane [7]; the foci of the lenslets are imaged onto a camera sensor [Fig. 1(A)]. To enable direct, quantitative comparison of our technique to more established methods, our microscope is designed to offer seamless switching to light-sheet (also known as selective-plane illumination microscopy; SPIM) or wide-field LFM modes [Supplement 1, Section 1, and Figs. S1-S2].

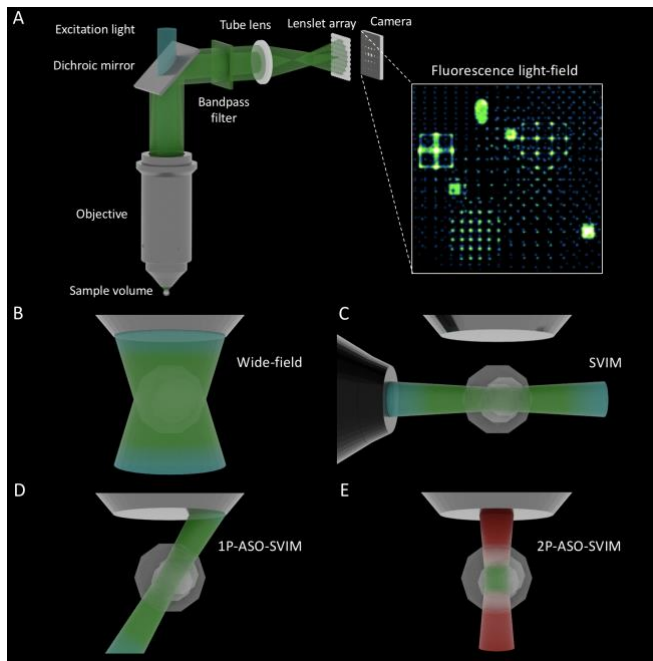


Fig. 1. Axial single-objective selective-volume illumination (ASO-SVIM). (A) Simplified schematic of light-field microscopy (LFM). Fluorescence light is collected from the sample volume by an objective lens, separated and filtered from the excitation light by the appropriate dichroic mirror and bandpass filter, and focused by a tube lens at an intermediate image plane where a lenslet array is positioned. The lenslet array refocuses the light onto a camera, so that each position in the 3D sample volume is mapped onto the camera as a unique light intensity pattern. The fluorescence light-field illustrated was captured with point-sources located at, above, and below the native focal plane. Such light-fields can be reconstructed to full volumes by solving the inverse problem [3]. (B) LFM with conventional wide-field illumination is compatible with standard forms of sample preparation but excites regions outside of the volume of interest (VOI). (C) Inspired by light-sheet microscopy (SPIM), SVIM selectively illuminates the VOI using orthogonal illumination and detection objectives. Shown previously [1-3], SVIM reduces background fluorescence outside of the VOI, increasing image resolution and contrast. (D, E) ASO-SVIM preferentially excites the VOI and collects the fluorescence using a single objective lens, providing flexibility in sample mounting similar to traditional microscopy. (D) 1P-ASO-SVIM uses an oblique light sheet, that is scanned in 1D, to define the excitation volume. (E) 2P-ASO-SVIM uses nonlinear excitation of a pulsed near-infrared (NIR) beam that is raster-scanned to define the VOI. In each figure, 1P excitation is depicted in cyan (A-D) and 2P excitation in red (E); fluorescence emission is depicted in green.

See also Supplement 1, Section 1, and Figs. S1-S2.

We benchmarked ASO-SVIM performance by measuring the point-spread function (PSF) with 175-nm fluorescent beads suspended in agarose. After 3D deconvolution [7,8], we obtained volumetric images with the expected maximum resolution, consistent with the optical design: $2.4 \pm 0.3 \mu\text{m}$ lateral full-width at half-maximum (FWHM); $5.7 \pm 0.2 \mu\text{m}$ axial FWHM [Supplement 1, Fig. S3(C)]. Due to diffraction and non-uniform sampling of the light-field volume [7,8], the 3D resolution was depth-dependent (varying up to $\sim 46\%$ over range of $z = -50$ to $50 \mu\text{m}$) [Supplement 1, Fig. S3(B)], and reconstructions contained grid-like artifacts near the native focal plane, as previously reported [7]. To reduce such artifacts in the reconstructions presented here, we applied a low-pass filter in Fourier space (k -space), truncating spurious spatial frequencies beyond the resolution limit of the native focal plane (Supplement 1, Section 2, Figs. S4-S5). The simple process of k -space filtering across the nominal focus dampened the artifacts and improved visualization of the 3D reconstructions, without any major loss of 3D resolution or spatial information (Supplement 1, Figs. S5-S6).

To test ASO-SVIM on biological samples, we imaged the vasculature of live larval zebrafish (at 5 days post-fertilization, dpf), labeled with green fluorescent protein (GFP). Zebrafish embryos and larvae are ideal for studies involving multicellular and multiscale imaging because of their small size, transparency, and amenability to genetic engineering. As expected, ASO-SVIM, using either 1P or 2P excitation, produced less out-of-volume background than did wide-field illumination [Fig. 2(A)], and this reduced background fluorescence yields higher contrast images, as we previously reported for SVIM [1,3]. This is clearly revealed in an x - z slice through the 3D volume [Fig. 2(A), bottom]. Although ASO-SVIM reconstructed images all fell short of the quality of the ground truth images (a deconvolved SPIM image stack), all three dimensions were acquired simultaneously, generating the 3D image more than 100-fold faster.

To obtain quantitative measures of the enhanced performance of 1P-ASO-SVIM and 2P-ASO-SVIM, we calculated the image contrast (defined as the standard deviation of the pixel intensities normalized to the mean intensity) for each x - y image plane [Fig. 2(B)]: 1P-ASO-SVIM showed a modest improvement; 2P-ASO-SVIM showed more dramatic improvement over wide-field LFM. Intensity profiles of LFM images [along the dashed yellow line in Fig. 2(A), bottom] documented the improved performance of ASO-SVIM [Fig. 2(C)], as did Fourier transforms of the images [Fig. 2(D,E)]. Thus, the reduction in background fluorescence substantially boosts image contrast as well as effective spatial resolution, both laterally and axially [Fig. 2(D,E) and Supplement 1, Fig. S7]. The enhanced contrast and effective resolution of the ASO-SVIM modalities are further demonstrated by comparing recorded images of single blood vessels, as well as measurements of the width of these vessels from the line profiles (Fig. 2(F,G) and Supplement 1, Fig. S8).

To test ASO-SVIM on a more demanding application, we recorded the activity of large populations of neurons in larval zebrafish. Imaging the nervous system in action within the intact brain is challenging because it requires cellular resolution over thousands of cells with sufficient temporal resolution to capture the transient firing of neurons. LFM is an attractive technique to meet these neuroimaging challenges because it can synchronously capture large volumes; however, the high level of background fluorescence in wide-field LFM has remained an impediment to efforts aimed at capturing brain-wide activity with cellular resolution [8,10-16]. We previously showed that the improved contrast and effective resolution of SVIM improved brain-wide functional imaging over conventional LFM [3]. We extended the demonstration and analysis to our new ASO-SVIM approach here.

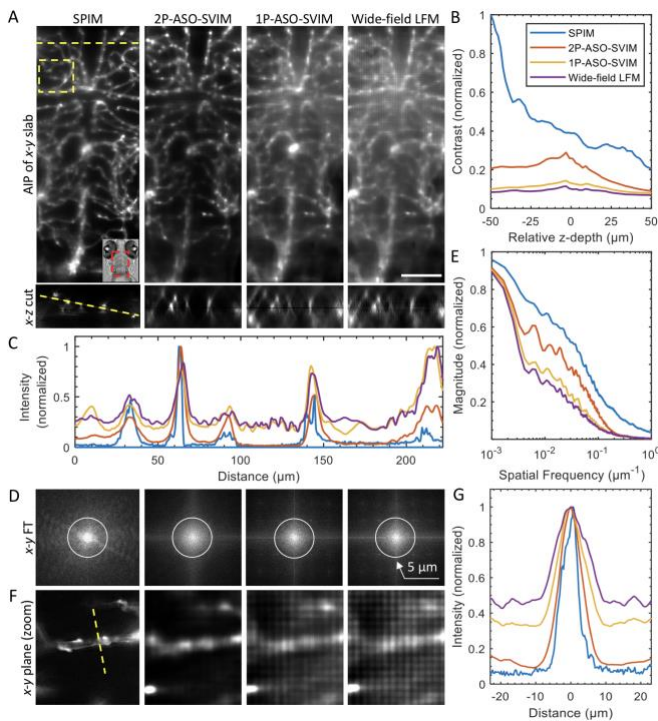


Fig. 2. ASO-SVIM improves contrast and effective resolution in live imaging of zebrafish larvae.

(A, Top) Average-intensity projections (AIPs) of a 100- μm -thick 3D image stack from the same transgenic [Tg(kdrl:GFP)] 5-dpf zebrafish, where the vasculature was fluorescently labeled, captured by different imaging modalities.

(Inset) Transmitted light image of the zebrafish head, where the dashed red rectangle marks the 230 μm \times 600 μm \times 100 μm volume imaged.

(Bottom) Cross-sectional (x - z) views at the location indicated by the dashed yellow line (top left, SPIM panel).

The SPIM volume consisted of 67 optical sections, collected serially over \sim 44 s; the LFM-based volumes were reconstructed from a single image with an exposure of 355 ms. Scale bar, 100 μm .

(B) Quantification of image contrast versus z -depth, showing improvements of 1P-ASO-SVIM and 2P-ASO-SVIM over wide-field LFM. Image contrast, measured as the standard deviation of the pixel intensities divided by the mean intensity, is plotted for each x - y slice, normalized by the value of the deconvolved SPIM (blue trace) at $z = -50$ μm .

(C) Intensity profiles along the same line for all four modalities (dashed yellow line shown on the x - z cut in A, bottom, SPIM). The fluorescence intensities of ASO-SVIM better agree with the ground truth SPIM data than does wide-field LFM.

(D) Fourier transforms (FTs) of x - y MIPs through the 100- μm -thick slabs in (A). Resolution bands (white circles) help show the increased spatial frequency content of ASO-SVIM compared to wide-field LFM, where more signal intensity at larger radial position designates higher resolution captured.

(E) Average amplitudes along k_y direction of the FTs shown in (D), showing that ASO-SVIM frequency spectra fall slower to the experimental noise floor, indicating better effective resolution than wide-field LFM. See also Supplement 1, Fig. S7.

(F) Enlarged x - y slices to highlight single blood vessels, centered at \sim 86 μm into the specimen, from the subregion indicated by dashed yellow box in (A, top left).

(G) Intensity profiles, averaged from the dashed yellow line shown in (F) and from 2 other similar vessel structures (Supplement 1, Fig. S8),

demonstrate the improvements in effective resolution of ASO-SVIM over wide-field LFM, in measuring the width of blood vessels.

To permit direct comparisons between modalities, we used 1P-ASO-SVIM, 2P-ASO-SVIM, and wide-field LFM to image the spontaneous brain activity of the same 5-dpf zebrafish, labeled with a genetically encoded pan-neuronal fluorescent calcium indicator [Fig. 3]. The reconstructed 4D recordings are compared by taking the standard deviation along the temporal axis [Fig. 3(A)], to highlight their capability in capturing active neurons, whose transient firings would produce voxels that have large intensity variation in time and thus appear as high-contrast puncta in the resulting projections. We calculated the image contrast of these temporal-standard-deviation projections: 2P-ASO-SVIM achieved the highest contrast, followed by the 1P ASO-SVIM, and then by wide-field LFM [Fig. 3(B)], suggesting that the ASO-SVIM modalities excel in capturing neuronal activity over wide-field LFM.

To quantitatively compare the performance of the different modalities in capturing brain activity at cellular resolution, we identified neurons in the 4D recordings by spot-segmenting the temporal-standard-deviation projections. This standard protocol [3] produced spatial masks corresponding to neurons that were active during the time-lapse. These masks were then applied to the 4D datasets to extract temporal signals that represent single-neuron activity traces [Fig. 3(C)]. The improved contrast of 2P-ASO-SVIM and 1P-ASO-SVIM allowed us to detect a greater number of active neurons in the brain compared to conventional wide-field illumination [Fig. 3(C)]. 2P-ASO-SVIM captured the largest number of active neurons, due not only to its higher contrast than its 1P counterpart (expanded below) but also because the NIR excitation light is invisible to the fish and thereby significantly reduces the response of the animal's visual system to the illumination, which would otherwise cloud spontaneous activity [3]. 2P-ASO-SVIM is thus an optimal tool for studies of visually sensitive neural behaviors.

1P-ASO-SVIM and 2P-ASO-SVIM offer distinct strengths. 1P-ASO-SVIM commands lower laser costs, and offers optical simplicity and exceptionally high volumetric acquisition speed, limited largely by the rate of the camera [3]. However, the 1P excitation volume is larger and intersects the sample obliquely [Fig. 1(D)], making 1P-ASO-SVIM less efficient at reducing background than SVIM. Like all forms of linear excitation, visible 1P excitation light increasingly scatters with depth, resulting in unavoidable background from outside the volume of interest. 2P-ASO-SVIM effectively eliminates background from out-of-volume fluorescence [Fig. 2(a)] due to nonlinear excitation: The quadratic dependence of 2P-excited fluorescence on the laser intensity restricts the excitation volume to near the focus [3,9], resulting in negligible background even with single-objective designs. The NIR excitation light is scattered much less than visible wavelengths, and any scattered light is unlikely to generate background as it is unlikely to achieve the intensity required to excite fluorescence or autofluorescence in tissue. Through the judicious selection of illumination NA and beam-scanning, it is straightforward to match the 2P excitation volume to the desired light-field region of interest (Supplement 1, Section 1). This advantage is partially tempered by the reduced speed of 2P-ASO-SVIM, as it requires scanning the excitation beam in 2D to achieve optimal excitation [9]. Potential slowing results from the lower 2P excitation cross section for almost all labels; increasing the intensity of the ultrafast laser cannot compensate for this, out of concern for photodamage, as discussed in [3].

As a final example of the combination of high-contrast, ultrahigh-speed volumetric imaging at cellular resolution and the sample-mounting flexibility of ASO-SVIM, we imaged 3D blood flow in nearly the entire larval zebrafish brain, covering a 670 μm \times 470 μm \times 200 μm volume at \sim 50 Hz, in 9 zebrafish mounted in a standard multi-well plate (Supplement 1, Fig. S9, and Visualizations 2-4). Together, our results show that ASO-SVIM offers a convenient middle ground between SPIM

and traditional wide-field LFM, offering improved contrast and effective resolution compared to LFM, while outperforming the 3D imaging speed of SPIM by approximately two orders of magnitude, as it requires only a single camera exposure to capture an extended volume. Compared to our earlier form of SVIM [1, 3], ASO-SVIM relaxes steric constraints by using only one objective, similar to recent developments in single-objective light-sheet-based microscopy [18-21], easing sample preparation and expanding the application space to multicellular systems that are impractical for a dual-objective design. Finally, the simplicity of ASO-SVIM renders it compatible and synergistic with many recent refinements of LFM [10-13], and we envision that together they will bring LFM-based imaging techniques into a wide range of biological systems and applications.

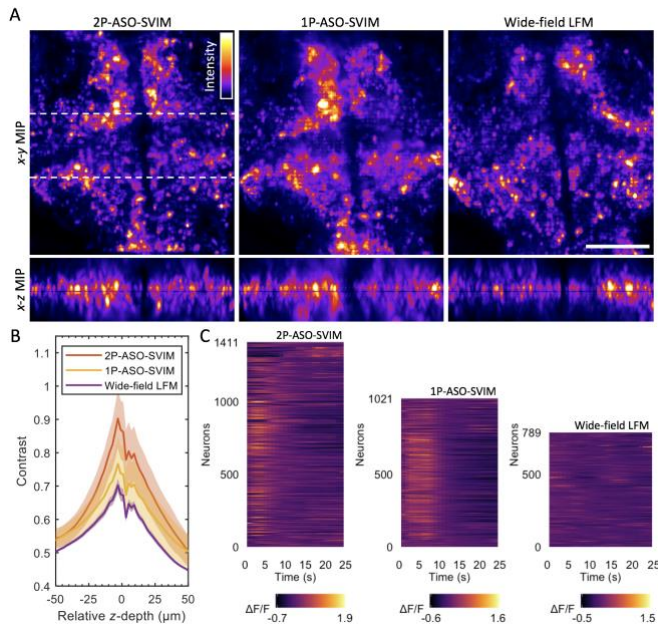


Fig. 3. ASO-SVIM enhances large-scale *in vivo* recording of neural activity in a $320 \mu\text{m} \times 350 \mu\text{m} \times 100 \mu\text{m}$ volume in larval zebrafish, at 5-dpf, Tg(elavl3:H2b-GCaMP6s). Volumetric rate of 1 Hz sufficiently captured the transient neuronal dynamics given the relatively slow temporal kinetics of the nuclear-localized calcium indicator GCaMP6s [17].

(A) MIPs of *x-y* (top) and *x-z* (bottom) brain-wide 100- μm -thick volumes of the same zebrafish. These projections depict the standard deviation over a 25-s period for each voxel, highlighting active neurons. Scale bar, 100 μm . See Visualization 1.

(B) Quantification of image contrast versus *z*-depth, showing progressive improvements of 1P-ASO-SVIM and 2P-ASO-SVIM over wide-field LFM. Means (center lines) and standard deviations (shadings) are shown.

(C) Single-neuron signal traces captured by the different modalities, extracted from the 4D datasets shown in (A). The greatest quantity of neurons were found with 2P-ASO-SVIM, followed by 1P-ASO-SVIM, and then wide-field LFM. See text for description of signal extraction protocol.

Funding. US National Science Foundation (1608744, 1650406, 1828793); US National Institutes of Health (1R01MH107238-01); Human Frontier Science Program (RGP0008/2017); Jet Propulsion

Laboratory Research Subcontract (1632330); Alfred E. Mann Doctoral Fellowship (to KKD).

Acknowledgment. We thank Dan Holland, Andrey Andreev, and Francesco Cutrale for insightful discussions.

Competing interests. TVT, SM, and SEF: patent application number PCT/US2017/019512 (pending).

See [Supplement 1](#) for supporting content.

REFERENCES

1. T.V. Truong, D.B. Holland, S. Madaan, A. Andreev, J.V. Troll, D.E.S. Koo, K. Keomanee-Dizon, M.J. McFall-Ngai, and S.E. Fraser, *bioRxiv* (2018).
2. N. Wagner, N. Norlin, J. Gierden, G. de Medeiros, B. Balázs, J. Wittbrodt, L. Hufnagel, and R. Prevedel, "Instantaneous isotropic volumetric imaging of fast biological processes," *Nat. Methods* **16**, 497 (2019).
3. T.V. Truong, D.B. Holland, S. Madaan, A. Andreev, K. Keomanee-Dizon, J.V. Troll, D.E.S. Koo, M.J. McFall-Ngai, and S.E. Fraser, *Comm. Biol.* **3**, 1 (2020).
4. W. Supatto, T.V. Truong, D. Débarre, E. Beaurepaire, *Cur. Op. Gen. Dev.* **21**, 538 (2011).
5. F. Cutrale, S.E. Fraser, and L.A. Trinh, *Annual Rev. of Biomed. Data Science* **2**, 223 (2019).
6. M. Levoy, R. Ng, A. Adams, M. Footer, and M. Horowitz, in *Proceedings of ACM SIGGRAPH* (ACM, 2006) p. 924.
7. M. Broxton, L. Grosenick, S. Yang, N. Cohen, A. Andalman, K. Deisseroth, and M. Levoy, *Opt. Express* **21**, 25418 (2013).
8. R. Prevedel, Y. G. Yoon, M. Hoffmann, N. Pak, G. Wetzstein, S. Kato, T. Schrödel, R. Raskar, M. Zimmer, E. S. Boyden, and A. Vaziri, *Nat. Methods* **11**, 727 (2014).
9. T.V. Truong, W. Supatto, D.S. Koos, J.M. Choi, and S.E. Fraser, *Nat. Methods* **8**, 757 (2011).
10. N.C. Pégard, H.Y. Liu, N. Antipa, M. Gerlock, H. Adesnik, and L. Waller, *Optica* **3**, 517 (2016).
11. L.M. Grosenick, M. Broxton, C.K. Kim, C. Liston, B. Poole, S. Yang, A.S. Andalman, E. Scharff, N. Cohen, O. Yizhar, C. Ramakrishnan, S. Ganguli, P. Suppes, M. Levoy, and K. Deisseroth, *bioRxiv*, 132688 (2017).
12. L. Cong, Z. Wang, Y. Chai, W. Hang, C. Shang, W. Yang, L. Bai, J. Du, K. Wang, and Q. Wen, *eLife* **6**, e28158 (2017).
13. T. Nöbauer, O. Skocek, A.J. Pernia-Andrade, L. Weilguny, F.M. Traub, M.I. Molodtsov, and A. Vaziri, *Nat. Methods* **14**, 811 (2017).
14. O. Skocek, T. Nöbauer, L. Weilguny, F.M. Traub, C.N. Xia, M.I. Molodtsov, A. Grama, M. Yamagata, D. Aharoni, D.D. Cox, P. Golshani, and A. Vaziri, *Nat. Methods* **25**, 429 (2018).
15. S. Aimon, T. Katsuki, T. Jia, L. Grosenick, M. Broxton, K. Deisseroth, T.J. Sejnowski, and R.J. Greenspan, *PLoS Biol.* **17**, e2006732 (2019).
16. Q. Lin, J. Manley, M. Helmreich, F. Schlumm, J.M. Li, D.N. Robson, F. Engert, A. Schier, T. Nöbauer, and A. Vaziri, *Cell* **180**, 536 (2020).
17. T.-W. Chen, T. J. Wardill, Y. Sun, S. R. Pulver, S. L. Renninger, A. Baohan, E. R. Schreier, R. A. Kerr, M. B. Orger, V. Jayaraman, L. L. Logger, K. Svoboda, and D. S. Kim, *Nature* **499**, 295 (2013).
18. V. Voleti, K.B. Patel, W. Li, C.P. Campos, S. Bharadwaj, H. Yu, C. Ford, M.J. Casper, R.W. Yan, W. Liang, C. Wen, K.D. Kimura, K.L. Targoff, E.M.C. Hillman, *Nat. Methods* **16**, 1054 (2019).
19. B. Yang, X. Chen, Y. Wang, S. Feng, V. Pessino, N. Stuurman, N.H. Cho, K.W. Cheng, S.J. Lord, L. Xu, D. Xie, R.D. Mullins, M.D. Leonetti, and B. Huang, *Nat. Methods* **16**, 501 (2019).
20. J. Kim, M. Wojcik, Y. Wang, S. Moon, E.A. Zin, N. Marnani, Z.L. Newman, J.G. Flannery, K. Xu, and X. Zhang, *Nat. Methods* **16**, 853 (2019).
21. E. Sapoznik, B.J. Chang, R.J. Ju, E.S. Wolf, D. Broadbent, A.F. Carisey, S.J. Stehbens, K.M. Lee, A. Marín, A.B. Hanker, J.C. Schmidt, C.L. Arteaga, B. Yang, R. Kruthoff, D.P. Shepherd, A. Millett-Sikking, A.G. York, K.M. Dean, R. Fiolka, *bioRxiv* 030569 (2020).

REFERENCES

1. T.V. Truong, D.B. Holland, S. Madaan, A. Andreev, J.V. Troll, D.E.S. Koo, K. Keomanee-Dizon, M.J McFall-Ngai, and S.E. Fraser, bioRxiv 403303 (2018).
2. N. Wagner, N. Norlin, J. Gierten, G. de Medeiros, B. Balázs, J. Wittbrodt, L. Hufnagel, and R. Prevedel, "Instantaneous isotropic volumetric imaging of fast biological processes," *Nature Methods* **16**, 497–500 (2019).
3. T.V. Truong, D.B. Holland, S. Madaan, A. Andreev, K. Keomanee-Dizon, J.V. Troll, D.E.S. Koo, M.J McFall-Ngai, and S.E. Fraser, "High-contrast, synchronous volumetric imaging with selective volume illumination microscopy," *Communications Biology* **3**, 1-8 (2020).
4. W. Supatto, T.V. Truong, D. Débarre, E. Beaurepaire, "Advances in Multiphoton Microscopy for Imaging Embryos," *Cur. Op. Gen. Dev.* **21**, 538-548 (2011).
5. F. Cutrale, S.E. Fraser, and L.A. Trinh, "Imaging, Visualization, and Computation in Developmental Biology," *Annual Review of Biomedical Data Science* **2**, 223-251 (2019).
6. M. Levoy, R. Ng, A. Adams, M. Footer, and M. Horowitz, "Light field microscopy," in *Proceedings of ACM SIGGRAPH (ACM, 2006)* p. 924-934.
7. M. Broxton, L. Grosenick, S. Yang, N. Cohen, A. Andalman, K. Deisseroth, and M. Levoy, "Wave optics theory and 3-D deconvolution for the light field microscope," *Optics Express* **21**, 25418-25439 (2013).
8. R. Prevedel, Y. G. Yoon, M. Hoffmann, N. Pak, G. Wetzstein, S. Kato, T. Schrödel, R. Raskar, M. Zimmer, E. S. Boyden, and A. Vaziri, "Simultaneous whole-animal 3D imaging of neuronal activity using light-field microscopy," *Nature Methods* **11**, 727-730 (2014).
9. T.V. Truong, W. Supatto, D.S. Koos, J.M. Choi, and S.E. Fraser, "Deep and fast live imaging with two-photon scanned light-sheet microscopy," *Nature Methods* **8**, 757-760 (2011).
10. N.C. Pégard, H.Y. Liu, N. Antipa, M. Gerlock, H. Adesnik, and L. Waller, "Compressive light-field microscopy for 3D neural activity recording," *Optica* **3**, 517-524 (2016).
11. L.M. Grosenick, M. Broxton, C.K. Kim, C. Liston, B. Poole, S. Yang, A.S. Andalman, E. Scharff, N. Cohen, O. Yizhar, C. Ramakrishnan, S. Ganguli, P. Suppes, M. Levoy, and K. Deisseroth, "Identification of cellular-activity dynamics across large tissue volumes in the mammalian brain," bioRxiv, 132688 (2017).
12. L. Cong, Z. Wang, Y. Chai, W. Hang, C. Shang, W. Yang, L. Bai, J. Du, K. Wang, and Q. Wen, "Rapid whole brain imaging of neural activity in freely behaving larval zebrafish (*Danio rerio*)," *eLife* **6**, e28158 (2017).
13. T. Nöbauer, O. Skoček, A.J. Pernía-Andrade, L. Weiglun, F.M. Traub, M.I. Molodtsov, and A. Vaziri, "Video rate volumetric Ca²⁺ imaging across cortex using seeded iterative demixing (SID) microscopy," *Nature Methods* **14**, 811-818 (2017).
14. O. Skoček, T. Nöbauer, L. Weiglun, F.M. Traub, C.N. Xia, M.I. Molodtsov, A. Grama, M. Yamagata, D. Aharoni, D.D. Cox, P. Golshani, and A. Vaziri, "High-speed volumetric imaging of neuronal activity in freely moving rodents," *Nature Methods* **25**, 429-432 (2018).
15. S. Aimon, T. Katsuki, T. Jia, L. Grosenick, M. Broxton, K. Deisseroth, T.J. Sejnowski, and R.J. Greenspan, "Fast near-whole-brain imaging in adult *Drosophila* during responses to stimuli and behavior," *PLoS Biology* **17**, e2006732 (2019).
16. Q. Lin, J. Manley, M. Helmreich, F. Schlumm, J.M. Li, D.N. Robson, F. Engert, A. Schier, T. Nöbauer, and A. Vaziri, "Cerebellar Neurodynamics Predict Decision Timing and Outcome on the Single-Trial Level," *Cell* **180**, 536-551 (2020).
17. T.-W. Chen, T. J. Wardill, Y. Sun, S. R. Pulver, S. L. Renninger, A. Baohan, E. R. Schreiter, R. A. Kerr, M. B. Orger, V. Jayaraman, L. L. Logger, K. Svoboda, and D. S. Kim, "Ultrasensitive fluorescent proteins for imaging neuronal activity," *Nature* **499**, 295–300 (2013).
18. V. Voleti, K.B. Patel, W. Li, C.P. Campos, S. Bharadwaj, H. Yu, C. Ford, M.J Casper, R.W. Yan, W. Liang, C. Wen, K.D. Kimura, K.L Targoff, E.M.C. Hillman, "Real-time volumetric microscopy of in vivo dynamics and large-scale samples with SCAPE 2.0," *Nature Methods* **16**, 1054-1062 (2019).
19. B. Yang, X. Chen, Y. Wang, S. Feng, V. Pessino, N. Stuurman, N.H. Cho, K.W. Cheng, S.J. Lord, L. Xu, D. Xie, R.D. Mullins, M.D. Leonetti, and B. Huang, "Epi-illumination SPIM for volumetric imaging with high spatial-temporal resolution," *Nature Methods* **16**, 501-504 (2019).
20. J. Kim, M. Wojcik, Y. Wang, S. Moon, E.A. Zin, N. Marnani, Z.L. Newman, J.G. Flannery, K. Xu, and X. Zhang, "Oblique-plane single-molecule localization microscopy for tissues and small intact animals," *Nature Methods* **16**, 853-857 (2019).
21. E. Sapozhnik, B.J Chang, R.J. Ju, E.S. Welf, D. Broadbent, A.F. Carisey, S.J. Stehbins, K.M. Lee, A. Marin, A.B. Hanker, J.C. Schmidt, C.L. Arteaga, B. Yang, R. Kruthoff, D.P. Shepherd, A. Millett-Sikking, A.G. York, K.M. Dean, R. Fiolka, "A Single-Objective Light-Sheet Microscope with 200 nm-Scale Resolution." bioRxiv 030569 (2020).